

Symmetry protection and large Fermi arcs in double Weyl semimetal CoGe

Chanchal K. Barman,^{1,*} Chiranjit Mondal,^{2,*} Sumiran Pujari,¹ Biswarup Pathak,^{2,3,†} and Aftab Alam^{1,‡}

¹*Department of Physics, Indian Institute of Technology, Bombay, Powai, Mumbai 400076, India*

²*Discipline of Metallurgy Engineering and Materials Science, IIT Indore, Simrol, Indore 453552, India*

³*Discipline of Chemistry, School of Basic Sciences, IIT Indore, Simrol, Indore 453552, India*

(Dated: November 16, 2021)

Unlike the two-fold Weyl fermions that are of significant theoretical and experimental interest presently, higher-fold chiral fermionic states have very recently been theoretically predicted in crystalline systems using symmetry arguments and Density Functional calculations. Here, we focus on such excitations in a few binary/ternary alloys (CoGe being the titular example), that belongs to space group (SG) 198. We found distinct three-fold, four-fold and six-fold chiral fermions in the bulk. We provide symmetry arguments for the protection of these degeneracies at high symmetry points in the Brillouin zone (BZ), with special emphasis on the four-fold fermions for spinless (at R point in the BZ) and spinfull (at Γ point) cases. Our surface simulations show that the size of Fermi arcs resulting from these chiral fermions are large, robust and untouched from the bulk states due to the near absence of bulk Fermi pockets. Spin-momentum locking in the presence of spin-orbit interaction is observed on the surface Fermi arcs. All these rich topological features make CoGe a promising candidate for future photo-emission and transport measurements.

Introduction: The discovery of chiral fermions in solid state quantum materials has kick-started a recent revolution in the field of condensed-matter physics. A methodological approach towards the understanding and search of new topological semimetals is to examine how crystalline symmetries in a material enforce or “symmetry-protect” the degenerate band-crossing points.^{1,2} These new type of quasiparticles³⁻⁶ in the solid state⁷⁻¹⁷ may not even have elementary particle counterparts.

Some of the new, unexpected excitations predicted recently are spin-1,¹⁵⁻¹⁸ charge-2 Dirac,^{17,18} and spin- $\frac{3}{2}$ chiral fermionic excitations. In three dimensional (3D) lattices, the well-known two-fold Weyl chiral fermions can be present in the absence of either the parity inversion (\mathcal{P}) or time reversal (\mathcal{T}) symmetry. They are characterized by non-zero topological charges called Chern numbers $C=\pm 1$.^{5,6} These Weyl fermions can be described by an effective spin- $\frac{1}{2}$ Hamiltonian $H \propto \hbar \delta \vec{k} \cdot \vec{\sigma}$ at lowest order. $\delta \vec{k}$ is small deviations from Weyl node in momentum space. $\vec{\sigma} \equiv \{\sigma_x, \sigma_y, \sigma_z\}$ are the 2×2 Pauli matrices. However, certain symmetries can also protect spin-1 or spin- $\frac{3}{2}$ chiral fermions^{17,18} that are three-fold and four-fold respectively. Their effective low-energy Hamiltonians are $H \propto \hbar \delta \vec{k} \cdot \vec{L}$, where L_i 's are (3×3) spin-1 and (4×4) spin- $\frac{3}{2}$ rotation generators respectively. The low energy dispersions follow from the corresponding model Hamiltonians, e.g. spin-1 fermions possess a combination of a Dirac-type linear band crossing and a flat band, as shown in Fig. 1(a), with $C=\pm 2$ and 0 respectively.

Additionally, two identical copies of spin- $\frac{1}{2}$ Weyl nodes can also be symmetry-protected.^{16,18} This leads to $C = \pm 2$ with four-fold degeneracy. The effective Hamiltonian for such a “multi-Weyl” node^{16,18} can be described as $H \propto \hbar \delta \vec{k} \cdot \vec{\sigma} \otimes \mathbb{I}_{2 \times 2}$, which are also called charge-2 Dirac nodes. The schematic diagram of low energy dispersions for Dirac, Weyl, spin-1 and charge-2 Dirac

nodes are shown in Fig. 1(a). The symmetry-protected band-crossings which carry $C=\pm 2$ are referred to as double Weyl nodes. These band-crossings are topologically robust under infinitesimal changes of the Hamiltonian parameters²² and lead to quite interesting phenomena.⁶

In the search for such multi-Weyl systems, there have been few studies on binary transition metal silicides (in SG 198) which are predicted to be double Weyl semimetals.¹⁵⁻²¹ Here, we focus on the experimentally synthesizable binary alloy CoGe,²⁴ which is a representative of the Germanide family. We provide a detailed analysis including *ab initio* simulations of bulk and surface excitations and symmetry protection arguments for the various multi-fold degeneracies. Unlike other reports, our symmetry arguments are not limited to binary AB

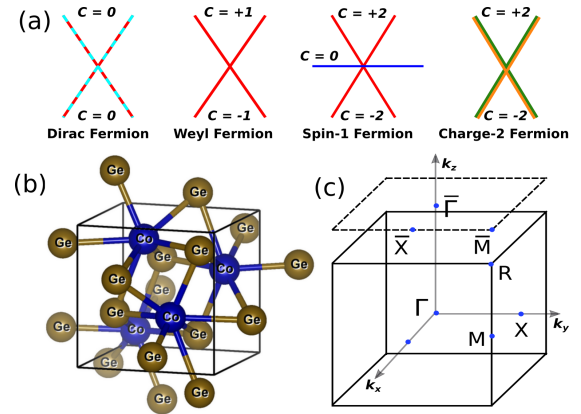


FIG. 1. (Color online) (a) Schematic band structure of Dirac, Weyl, Spin-1 and Charge-2 fermion. (b) Unit Cell of CoGe structure (space group P213). (c) Bulk Brillouin zone (BZ) and (001) surface BZ (represented by dashed square). The high symmetry points are shown in the BZ.

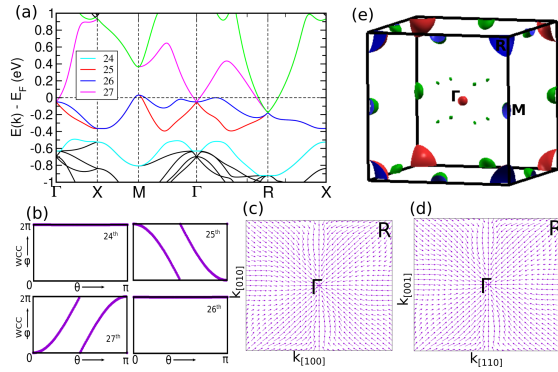


FIG. 2. (Color online) (a) Electronic structure of CoGe without spin-orbit interaction (SOI). Length in (a) gives different band index. (b) Evolution of Wannier charge center (WCC) around a spherical surface enclosing the three-fold degeneracy at Γ point calculated for different bands (24^{th} to 27^{th}). This is shown as a representative example of Chern number computations for all the multi-fold band crossings. θ, ϕ are the usual spherical coordinates. (c,d) Berry Curvature plotted in $k_z=0$ (left) and $k_x=k_y$ (right) plane. (e) 3D Fermi surface in the cubic Brillouin zone of CoGe without SOI.

systems alone, and we will look at some non-binary systems as well. We performed *ab initio* electronic structure calculations using Vienna Ab-initio Simulation Package (VASP)^{25,26} with Perdew-Burke-Ernzerhof (PBE)²⁶ exchange correlation. Chern numbers were calculated using Wilson charge center (WCC) evolution of Maximally Localized wannier functions (MLWF)^{28–30} obtained from wannier90³¹. Surface spectra and Fermi arcs were simulated using iterative Green’s function method.^{32–34} Further information on computational details can be found in the supplementary.⁴⁴

Crystal structure Information: The crystal structure and the corresponding BZ for CoGe are shown in Fig. 1(b,c). CoGe crystallizes in cubic structure with SG $P2_13$ under high pressures.²⁴ The primitive cell contains four formula units with both Co and Ge atoms lying on threefold axes (which lie along the body diagonal), occupying the same Wyckoff sites 4a (x, x, x). The internal co-ordinates are $x_{Co} = 0.1359(9)$ and $x_{Ge} = 0.8393(7)$. The theoretically optimized lattice parameter of CoGe is found to be 4.64 Å which matches fairly well with experimental value, 4.637 Å.²⁴ Each Co(Ge) atom has primary coordination of seven Ge(Co) atoms at a distances of 2.385, 2.403 ($\times 3$) and 2.615 ($\times 3$) Å. The next-nearest neighbors of each Co atom are six Co atoms of equivalent type at a distance 2.846 Å. Similarly, each Ge atom is surrounded by six next-nearest neighbor of Ge atoms at a distance 2.881 Å. Though both Co and Ge occupy same Wyckoff sites, the position of second nearest neighbors subtly dictates the different coordination environment for both of them.

Symmetry Arguments: The crystal structure of CoGe has tetrahedral (T_4) point group symmetry with the

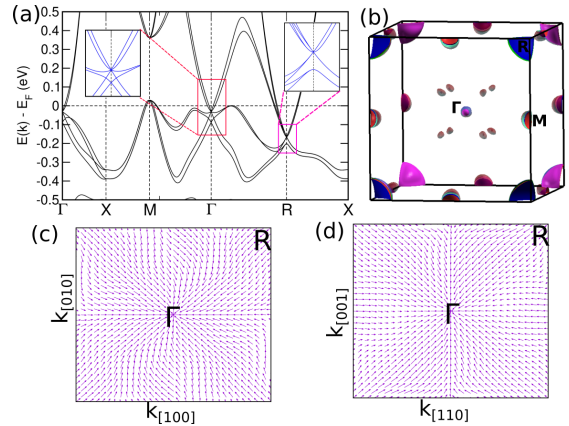


FIG. 3. (Color online) (a) Electronic structure of CoGe in the presence of SOI. The various degeneracies at the nodal points in this figure and in Fig. 2 are protected by non-symmorphic screw rotation, three fold rotation symmetries and time-reversal symmetry. (b) 3D Fermi surface at isolevel E_F . (c,d) Berry Curvature plotted in $k_z=0$ (left) and $k_x=k_y$ (right) plane highlighting its flows between R and Γ points in agreement with the sign of the topological charges.

following information germane to our analysis.³⁶ The point group has three generators at Γ point: two screws, $S_{2z} = \{C_{2z}|\frac{1}{2}, 0, \frac{1}{2}\}$, $S_{2y} = \{C_{2y}|0, \frac{1}{2}, \frac{1}{2}\}$ and a three-fold rotation $S_3 = \{C_{3,111}^+|0, 0, 0\}$. They satisfy $S_{2z}S_3 = S_3S_{2y}$ and $S_3S_{2z}S_{2y} = S_{2y}S_3$. Due to S_3 , the third screw symmetry $S_{2x} = \{C_{2x}|\frac{1}{2}, \frac{1}{2}, 0\}$ is also present. On the otherhand at the R point, the three generators are $S_{2x} = \{C_{2x}|\frac{1}{2}, \frac{3}{2}, 0\}$, $S_{2y} = \{C_{2y}|0, \frac{3}{2}, \frac{1}{2}\}$, and $S_3 = \{C_{3,111}^-|0, 1, 0\}$. They satisfy $S_{2x}S_3 = S_3S_{2y}$ and $S_3S_{2x}S_{2y} = S_{2y}S_3$.

We will start with the spinless case for which time reversal operator (\mathcal{T}) squares to identity (\mathbb{I}). At the Γ -point, the electronic structure can potentially show a three-fold band degeneracy. However, the Γ point symmetries do not necessarily imply three-fold degeneracies. For a three-fold degeneracy, the two screw symmetries S_{2y} and S_{2z} should *commute* and square to \mathbb{I} as is the case at Γ , as well as S_3 should act non-trivially ($S_3|\psi\rangle \neq |\psi\rangle$) where $|\psi\rangle$ is a simultaneous eigenstate of S_{2y} and S_{2z} ; see supplementary Sec. I.C of Ref. 3). It turns out that there can also be two-fold degeneracies or one-fold states at Γ point consistent with the symmetries if S_3 is trivial.

The symmetry properties at R point are crucially different. At this point, the two screws S_{2x} and S_{2y} now *anticommute* and square to $-\mathbb{I}$, and hence the previous three-fold degeneracy argument does not apply anymore. Ref. 18 offered an intuition that the degeneracy at R point has to be even dimensional with a lower bound of four.³⁷ From our analysis, we shall show that it has to be even with an upper bound of four in presence of S_3 .

Firstly, we can get a two-fold degeneracy using the anticommutation of the screws: $|\psi\rangle$ and $S_{2x}|\psi\rangle$ are distinct

eigenstates under S_{2y} , say with eigenvalues of i and $-i$ respectively without loss of generality. We can get a further two-fold degeneracy due to $S_{2z}S_3 = S_3S_{2y}$: $S_3|\psi\rangle$ and $S_{2y}S_3|\psi\rangle$ are distinct eigenstates now under S_{2x} with eigenvalues i and $-i$ respectively. If S_3 is non-trivial³⁸ and takes us out of the subspace of $|\psi\rangle$ and $S_{2x}|\psi\rangle$, i.e. minimally $\langle\psi|S_3|\psi\rangle = 0$, then mutual orthogonality of the two pairs is ensured.⁴¹ Time reversal (effectively complex conjugation) does not generate any new states for spinless electrons. Since we have accounted for all the symmetries present at R , we can at most get a symmetry-protected four-fold degeneracy and *no higher*. Combining with the argument of Ref. 18, we arrive at an *exactly* four-fold node protected by symmetries.

Going to the spinfull case for which $\mathcal{T}^2 = -\mathbb{I}$, the Kramer's degeneracies are lifted throughout the zone except at the time-reversal invariant momenta in presence of spin-orbit interaction, (SOI) because the crystal does not possess space-inversion symmetry. Adding the spin quantum number to a potential three-fold spinless degeneracy at Γ , we would like to understand what happens to the six states under SOI. It turns out that they can not give rise to a six-fold degeneracy, but at least have to split into two nodal points with four-fold degenerate and two-fold degenerate states. This is because only a four-fold degeneracy can at most be protected by Γ point symmetries. The reason for this is that now the screws S_{2y} and S_{2z} anticommute (and square to $-\mathbb{I}$) at Γ point instead of R point for the spinless case.³⁹ Thus, we can again get a four-fold degeneracy by the argument previously made for the spinless case at R point. However, for spinfull case, time reversal could potentially generate new eigenstates. But, *mutual* orthogonality of S_{2y} and S_{2z} eigenstates and their time-reversed partners is *not* ensured due to imaginary eigenvalues under the screws.⁴¹ Thus, we can only conclude a four-fold degeneracy and no higher. This completes the splitting argument. Also, a single-fold spinless band at Γ (if S_3 is trivial) will give rise to Kramer's two-fold degeneracy in the spinfull case. Similarly, a four-fold spinfull degeneracy arising from a two-fold spinless degeneracy is also consistent with the symmetries. On the other hand, at R point there can be six-fold degeneracies.³

To explain the spinfull four-fold degeneracy at the Γ point for AB systems, an alternate "top-down" argument was given in Ref. 15. Chang *et al* started with a eight dimensional representation of the Hamiltonian after making (minimal) assumptions on the nature of the orbitals in the unit cell. They then wrote down the distinct symmetry allowed "mass" terms in the $\mathbf{k} \cdot \mathbf{p}$ Hamiltonian based on the procedure laid down in Ref. 40 to reduce down to a four-fold degeneracy. Our arguments⁴¹ above are rather "bottom-up" and purely based on symmetries of the SG. On the other hand, comparing with the arguments of Ref. 3 for the case of commuting screws, we have paid attention to the interplay of S_3 symmetry of SG 198 with anticommuting screws which forbids any degeneracies higher than four-fold (and *only* four-fold for

spinless case at R point). In particular, our arguments also predict that systems beyond AB class, e.g. ternaries in SG 198 will also host these four-fold degeneracies.

We finally note that the four-fold degeneracies at R point have charge-2 Dirac nodal character. This is ensured because of the presence of two-fold line degeneracies along R - X and M - X directions (in fact, the whole $k_x = \pi$ and symmetry-related planes). Such additional symmetry protection obtains from a product of time reversal and screw symmetries (e.g. $\mathcal{T}S_{2x}$)⁴¹ leading to Kramer's-like two-fold degeneracies. Four-fold degeneracies at Γ point are not so constrained and thus have spin- $\frac{3}{2}$ character instead.

Bulk Excitations: Figure 2(a) shows the electronic band structure of CoGe in the absence of SOI. Different colored lines in Fig. 2(a) indicate band index (24 to 27). At Γ , we see a three-fold degeneracy as discussed earlier. There are also two-fold degeneracies and one-fold states at Γ at other energies (not highlighted). The shift of wannier charge centers at Γ -point for 24th-27th bands are shown in Fig. 2(b). Since the WCCs shift by -4π , 0 , 4π , the Chern number for 25th to 27th bands are $C(25)=-2$, $C(26)=0$ and $C(27)=+2$ respectively. These excitations are dubbed as spin-1 double Weyl excitations.

On the other hand at R point, we find *only* four-fold degeneracies in line with the symmetry arguments. One such four-fold degeneracy is highlighted in Fig. 2(b). Few more examples involving binary AB as well as ternary systems with the same SG are shown in the supplementary.⁴⁴ The calculated Chern number at this four-fold degenerate node (referred to as charge-2 Dirac node in Fig. 1 (a)) is ± 2 . Hence, the total Chern number is *zero* in the entire zone in accordance with the Nielsen-Ninomiya theorem.⁴² We further show the Berry curvature ($\tilde{\Omega}$) on $k_z=0$ and $k_x=k_y$ plane in Fig. 2(c,d) to highlight that it flows between R and Γ points in agreement with the sign of the topological charges. Figure 2(e) describes the 3D Fermi surface (FS) topology at isolevel E_F . The tiny sphere at the zone center arises due to electron-like Fermi pocket, as shown by magenta color band in Fig. 2(a). Along Γ - R direction, the Fermi level hardly touches the blue colored band. Near the corner of the zone, the red and blue surfaces of FS come from the doubly degenerate electron-like band at/around R point. A tiny hole-like Fermi pocket appears at M point as shown in Fig. 2(a,e).

Next, we include the effect of SOI into our calculations, and the results are shown in Fig. 3. At Γ , we get at most a four-fold degeneracy as dictated by symmetry arguments. One such four-fold degeneracy is highlighted in Fig. 3(a). Whereas at R -point, six-fold degeneracy is also allowed by symmetries as highlighted in Fig. 3(a). Figure 3(b) illustrates the Fermi surface (FS) map with SOI. At Γ point, two concentric spherical shape FSs are found, which arise from the four-fold spin-3/2 excitations. The bands in the inner(outer) sphere possess Chern number -1(-3). At R , FS corresponds to four electron-like bands

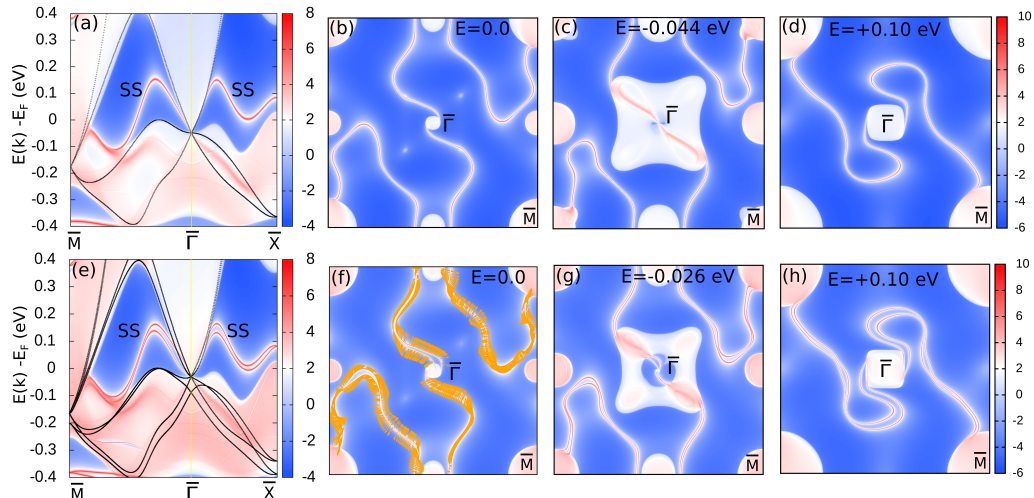


FIG. 4. (Color online) (a) and (e) Surface spectrum at side surface (001) without and with SOI respectively. Surface states are marked by SS. Superimposed bulk band structure along R - Γ - X are represented by black lines. (b-d) Fermi surface contour at energy window E_F (Fermi energy), $E_F - 0.44$ (spin-1 Weyl node) and $E_F + 0.1$ eV, without SOI. (f-h) Same as (b-d) but with SOI. (f) also shows the spin texture (yellow arrows) in presence of SOI.

from double spin-1 excitations with $C=\pm 2$. Along Γ - R and at M point in the BZ, tiny Fermi pockets are observed. Fig. 3(c,d) shows the berry curvature maps on $k_z=0$ and $k_x=k_y$ plane. This maps again confirm the flow of curvature between R and Γ . Notably, under ambient conditions, CoGe crystallizes in the SG $C2/m$,²³ where none of the above band topology is observed in our calculations.⁴⁴

Surface Excitations: Figure 4 shows the surface state results for these unconventional fermions. Fermi arcs on the surface, if present, are generally expected to connect topological nodes of opposite chirality. We studied the (001) surface in which R and Γ points fall at different locations (as shown in Fig. 1(c)), in contrast to (111) surface to allow for distinct arcs. Figure 4(a) shows the (001) surface spectrum for CoGe without including SOI. The Fermi arcs (FAs) spectral weights in absence of SOI are shown in Fig. 4(b-d) (see caption for different energy cuts.) A pair of FAs runs between the $\bar{\Gamma}$ point and \bar{R} point, as anticipated between the opposite Chern number multi-Weyl nodes.

Under the effect of SOI and consequent doubling of the Chern number ($|C| = 4$) at R and Γ point, the essential new feature involves two pairs of FA states that emerge from the bulk projected states at $\bar{\Gamma}$ and \bar{M} point, as clearly observed from the surface spectrum, as shown in Fig. 4(e). Furthermore, Fig. 4(f) reveals the spin-momentum-locked spin texture of the FAs when SOI is included. Without SOI, two doubly-spin-degenerate FAs appear. SOI lifts the spin-degeneracy everywhere except at time-reversal invariant momenta, and thus two pairs of FAs appear with anti-parallel spin polarization. Such spin polarized textures may offer promising applications in spintronics.^{45,46}

Conclusion: It is important to note that the Weyl nodes that appear in systems such as WTe_2 ,⁵ $MoTe_2$,⁴⁷ $LiAlGe$,⁴⁸ $TaAs(P)$,⁴⁹ $NbAs(P)$ ⁵⁰ and so on are accidental band crossings with the FAs relatively smaller in size. In contrast, the Γ and R point band-crossings in CoGe are robustly protected by the crystal space group symmetries. Also the FAs on the (001) surface in CoGe are much larger since the nodes are well-separated in BZ. Other promising feature of CoGe is the “clean” nature of FAs are because of the near absence of spectral weights from bulk states at E_F , as obvious from Fig. 4. This makes CoGe relatively superior than many other reported binary alloys (of SG # 198), such as $GaPt$,⁵² $GaPd$,⁵¹ $AlPd$,⁵³ $AlPt$,^{21,54} $RhGe$,⁵⁵ $AuBe$,⁵⁶ MSi ($M=Fe, Mn, Ru, Re$)¹⁸ which suffer from large spectral weight contributions of extra bulk band crossings across E_F . Very recently, experiments^{19,20} have borne out these advantages for the related compound $CoSi$,¹⁷ which is motivating for further experiments on CoGe which can be synthesized.²⁴

In summary, we predict an ideal higher Chern-number topological semimetal in CoGe in agreement with previous bulk studies on AB systems (with SG 198). This class of binary systems, in general, exhibit rich underlying symmetry gives rise to interesting topological properties. We gave new, alternate Kramer’s theorem-like arguments based on the inter-relationships between two non-symmorphic screws and three-fold rotations to explain the four-fold degeneracies at R for the spinless case (only possibility) and at Γ for the spinfull case. Large, clean Fermi arcs are predicted on the (001) surface for CoGe. The energy offset between spin-1 and the double Weyl nodes at Γ and R point makes this compound suitable for possible quantized circular photogalvanic effect with possibilities of technological applications.^{15,57} All

these promising features of CoGe attracts future experimental investigations to reconfirm the topological chiral semimetals with topological charges larger than $C=\pm 1$.

CKB acknowledges IIT Bombay for financial support in the form of teaching assistantship. CM acknowledges

MHRD-India for financial support. AA acknowledges DST-SERB (Grant No. CRG/2019/002050) for funding to support this research. SP acknowledges financial support from IRCC, IIT Bombay (17IRCCSG011) and SERB, DST, India (SRG/2019/001419).

-
- * These two authors have contributed equally to this work
 † biswarup@iiti.ac.in
 ‡ aftar@iitb.ac.in
- ¹ S. M. Young, S. Zaheer, J. C. Y. Teo, C. L. Kane, E. J. Mele, and A. M. Rappe, *Phys. Rev. Lett.* **108**, 140405 (2012).
 - ² Chen Fang, Matthew J. Gilbert, Xi Dai, and B. Andrei Bernevig, *Phys. Rev. Lett.* **108**, 266802 (2012).
 - ³ B. Bradlyn *et al.*, *Science* **353**, aaf5037 (2016)
 - ⁴ P.B. Pal, *Am. J. Phys.* **79**, 485 (2011).
 - ⁵ Alexey A. Soluyanov, Dominik Gresch, Zhijun Wang, QuanSheng Wu, Matthias Troyer, Xi Dai & B. Andrei Bernevig, *Nature* volume **527**, 495 (2015).
 - ⁶ N.P. Armitage, E.J. Mele, and Ashvin Vishwanath, *Rev. Mod. Phys.* **90**, 015001 (2018).
 - ⁷ C. K. Barman, Chiranjit Mondal, Biswarup Pathak, and Aftab Alam, *Phys. Rev. B* **99**, 045144 (2019).
 - ⁸ B.J. Wieder, Y. Kim, A.M. Rappe, and C.L. Kane, *Phys. Rev. Lett.* **116**, 186402 (2016).
 - ⁹ Chiranjit Mondal, C. K. Barman, Aftab Alam, and Biswarup Pathak, *Phys. Rev. B* **99**, 205112 (2019).
 - ¹⁰ B. Q. Lv *et al.*, *Nat. Lett.* **546**, 627 (2017).
 - ¹¹ R. Yu, H. Weng, Z. Fang, X. Dai, and X. Hu, *Phys. Rev. Lett.* **115**, 036807 (2015).
 - ¹² Y. Kim, B. J. Wieder, C. L. Kane, and A. M. Rappe, *Phys. Rev. Lett.* **115**, 036806 (2015).
 - ¹³ J.-T. Wang, H. Weng, S. Nie, Z. Fang, Y. Kawazoe, and C. Chen, *Phys. Rev. Lett.* **116**, 195501 (2016).
 - ¹⁴ G. Bian, *et al.*, *Nat. Commun.* **7**, 10556 (2016).
 - ¹⁵ Guoqing Chang, *et al.*, *Phys. Rev. Lett.* **119**, 206401 (2017).
 - ¹⁶ H. Miao, T.T. Zhang, L. Wang, D. Meyers, A.H. Said, Y.L. Wang, Y.G. Shi, H.M. Weng, Z. Fang, and M.P.M. Dean, *Phys. Rev. Lett.* **121**, 035302 (2018).
 - ¹⁷ Peizhe Tang, Quan Zhou, and Shou-Cheng Zhang, *Phys. Rev. Lett.* **119**, 206402 (2017).
 - ¹⁸ Tiantian Zhang, Zhida Song, A. Alexandradinata, Hongming Weng, Chen Fang, Ling Lu, and Zhong Fang, *Phys. Rev. Lett.* **120**, 016401 (2018).
 - ¹⁹ Daichi Takane *et al.*, *Phys. Rev. Lett.* **122**, 076402 (2019).
 - ²⁰ Daniel S. Sanchez *et al.*, *Nature* **567**, 500 (2019)
 - ²¹ Niels B. M. Schröter, Ding Pei, Maia G. Vergniory, Yan Sun, *et al.*, *Nat. Phys.* **15**, 759 (2019).
 - ²² The topological charges or Chern numbers being integral can not change continuously.
 - ²³ N. Audebrand, M. Ellner, and E. J. Mittemeijer, *Powder Diffr.* **15(2)** 120-122 (2000).
 - ²⁴ V.I. Larchev and S. V. Popova, *Journal of the Less-Common Metals* **87**, 53 (1982).
 - ²⁵ G. Kresse and J. Hafner, *Phys. Rev. B* **47**, 558(R) (1993)
 - ²⁶ G. Kresse and D. Joubert, *Phys. Rev. B* **59**, 1758 (1999)
 - ²⁷ P. E. Böchl, *Phys. Rev. B* **50**, 17953 (1994).
 - ²⁸ Nicola Marzari and David Vanderbilt, *Phys. Rev. B* **56**, 12847 (1997).
 - ²⁹ Ivo Souza, Nicola Marzari, and David Vanderbilt, *Phys. Rev. B* **65**, 035109 (2001).
 - ³⁰ Nicola Marzari, Arash A. Mostofi, Jonathan R. Yates, Ivo Souza, and David Vanderbilt, *Rev. Mod. Phys.* **84**, 1419 (2012).
 - ³¹ AA Mostofi, JR Yates, G Pizzi, YS Lee, I Souza, D Vanderbilt, N Marzari, *Comput. Phys. Commun.* **185**, 2309 (2014)
 - ³² D. H. Lee and J. D. Joannopoulos, *Phys. Rev. B* **23**, 4988 (1981).
 - ³³ D. H. Lee and J. D. Joannopoulos, *Phys. Rev. B* **23**, 4997 (1981).
 - ³⁴ M P Lopez Sancho, J M Lopez Sancho, J M L Sancho and J Rubio, *J. Phys. F:Met. Phys.* **15**, 851 (1985).
 - ³⁵ QuanSheng Wu, ShengNan Zhang, Hai-Feng Song, Matthias Troyer, Alexey A. Soluyanov, *Computer Physics Communications* **224**, 405 (2018).
 - ³⁶ *The Mathematical Theory of Symmetry in Solids: Representation Theory for Point Groups and Space Groups*, P. Cracknell and Christopher J. Bradley, ISBN: 9780199582587, Oxford: Clarendon Press, 1972.
 - ³⁷ Basically, the presence of three mutually anticommuting screws in presence of time-reversal symmetry can not admit two-fold (real) representations, but only four-fold or higher. (See pg. 2, column 2, bottom paragraph in Ref. 18)
 - ³⁸ A trivial S_3 , i.e. $S_3|\psi\rangle = |\psi\rangle$, is not allowed, since two anticommuting operators can not share a simultaneous eigenstate with non-zero eigenvalue. S_3 can not exchange $|\psi\rangle$ and $S_{2x}|\psi\rangle$ as well for the same reason. S_3 can however in principle create some linear combination of $|\psi\rangle$ and $S_{2x}|\psi\rangle$, in which case this argument would give a two-fold degeneracy.
 - ³⁹ This difference in screw commutation relations at Γ and R points is due to the different action of a 2π rotation for spinless and spinfull cases.
 - ⁴⁰ B. J. Wieder and C. L. Kane, *Phys. Rev. B* **94**, 155108 (2016).
 - ⁴¹ Verbose details are give in Supplemental Information.⁴⁴
 - ⁴² H. B. Nielsen and M. Ninomiya, *Phys. Lett.* **105B**, 219 (1981).
 - ⁴³ Xiangang Wan, Ari M. Turner, Ashvin Vishwanath, and Sergey Y. Savrasov, *Phys. Rev. B* **83**, 205101 (2011).
 - ⁴⁴ Supplemental information at [URL]. It contains auxiliary computational details, elaborations on the symmetry arguments presented concisely in the main text, and supplementary evidence from other binary/ternary systems.
 - ⁴⁵ Yoshinori Tokura, Kenji Yasuda & Atsushi Tsukazaki, *Nature Reviews Physics* **1**, 126-143 (2019).
 - ⁴⁶ S.D. Bader and S.S.P. Parkin, *Annu. Rev. Condens. Matter Phys.* **2010**. 1:7188
 - ⁴⁷ Lunan Huang, Timothy M. McCormick, Masayuki Ochi, *et al.*, *Nat. Mat.* **15**, 1155 (2016).
 - ⁴⁸ Su-Yang Xu, Nasser Alidoust, Guoqing Chang *et al.*, *Science Advances*, **3(6)**, e1603266 (2017).

- ⁴⁹ Hongming Weng, Chen Fang, Zhong Fang, B. Andrei Bernevig, and Xi Dai *Phys. Rev. X* **5**, 011029 (2015).
- ⁵⁰ S.-M. Huang, S.-Y. Xu et al., *Nat. Commun.* **6**, 7373 (2015).
- ⁵¹ E. Hellner and F. Laves, *Zeitschrift Naturforschung Teil A* **2**, 177 (1947)
- ⁵² Marc Armbrüster, Horst Borrmann, Michael Wedel, Yurii Prots, Rainer Giedigkeit, Peter Gille, *Zeitschrift für Kristallographie - New Crystal Structures*, **225**(4), 617 (2014).
- ⁵³ M. Ettenberg, K. L. Komarek, and E. Miller, *Metallurgical Transactions* **2**, 1173 (1971).
- ⁵⁴ K. Schubert et al., *Naturwissenschaften* **43**, 248 (1956).
- ⁵⁵ V. Larchev and S. Popova, *Journal of the Less Common Metals* **87**, 53 (1982).
- ⁵⁶ Drew J. Rebar, Serena M. Birnbaum, John Singleton, Mojammel Khan, J. C. Ball, P. W. Adams, Julia Y. Chan, D. P. Young, Dana A. Browne, and J. F. DiTusa, *Phys. Rev. B* **99** 094517 (2019).
- ⁵⁷ Fernando de Juan, Adolfo G. Grushin, Takahiro Morimoto & Joel E Moore, *Nat. Commun.* **8**, 15995 (2017).

Supplementary Information for “Symmetry protection and large Fermi arcs in double Weyl semimetal CoGe”

Chanchal K. Barman,^{1,*} Chiranjit Mondal,^{2,*} Sumiran Pujari,¹ Biswarup Pathak,^{2,3,†} and Aftab Alam^{1,‡}

¹*Department of Physics, Indian Institute of Technology, Bombay, Powai, Mumbai 400076, India*

²*Discipline of Metallurgy Engineering and Materials Science, IIT Indore, Simrol, Indore 453552, India*

³*Discipline of Chemistry, School of Basic Sciences, IIT Indore, Simrol, Indore 453552, India*

(Dated: November 16, 2021)

This supplement contains auxiliary computational details, elaborations on the symmetry arguments presented concisely in the main text, and supplementary evidence from other binary/ternary systems. The computational details are given in Sec. I. Sec. II sets up the symmetry discussion. Sec. III is devoted to the band degeneracies at Γ and R point for spinless case. In Sec. IIIC, we have shown band structures of several other binary and ternary alloys which belong to same space group as CoGe. This provides additional corroboration on *exclusive* four-fold degeneracies at R point for any system that belongs to space group 198 in the absence of spin-orbit coupling. Sec. IV is devoted to the analysis of degeneracy for spinfull case. Sec. V explains the two-fold line-degeneracies along R - X and M - X high symmetry directions in the Brillouin Zone (BZ). In Sec. VI, we show the electronic structure for the case when CoGe crystallizes in space group $C2/m$ which has lower symmetry. Finally in Sec. VII for reasons of pedagogical completeness, we have presented a compendium of the demonstrations of various relations between the crystal symmetry operations that are exploited to symmetry-protect the various degeneracies.

I. COMPUTATIONAL DETAILS

The *ab-initio* calculations were performed with projected augmented-wave basis¹ with an energy cut off of 500 eV. Total energy (force) was converged upto 10^{-6} eV/cell (0.001 eV/Å). A $12 \times 12 \times 12$ Γ -centered k-mesh was used to perform the bulk Brillouin zone(BZ) integrations. The spin-orbit coupling (SOC) interaction was included self-consistently. Also as mentioned in the main text, Maximally Localized wannier functions (MLWF)²⁻⁴ were used to construct tight binding model Hamiltonian to closely reproduce the bulk band structure. The Chern numbers associated with the various multi-fold bands were calculated using the method of Wilson charge center (WCC) evolution implemented in wannier90 package.⁵ The spectral weights in Fermi arcs and surface spectrum were calculated using iterative Green’s function⁶⁻⁸ scheme implemented in WannierTools package.⁹

II. SOME PRELIMINARIES

Following usual conventions, we will specify any crystal symmetry operation by a point group operation \mathcal{O} followed by a translation, \vec{t} . For pure point group operations, $\vec{t} = (0, 0, 0)$. The rules of combining two crystal symmetry operations is:

$$\begin{aligned} \{\mathcal{O}_1|\vec{t}_1\}\{\mathcal{O}_2|\vec{t}_2\} &= \{\mathcal{O}_1\mathcal{O}_2|\mathcal{O}_1\vec{t}_2 + \vec{t}_1\} \\ \{\mathcal{O}|\vec{t}\}^{-1} &= \{\mathcal{O}^{-1} | -\mathcal{O}^{-1}\vec{t}\} \end{aligned}$$

Pure translations are indicated by $\{\mathbb{1}|\vec{t}\} = e^{-i\vec{k}\cdot\vec{t}}$, where $\mathbb{1}$ is an identity operation, and \vec{k} and \vec{t} are reciprocal wave vector and translation vector respectively. We use \mathcal{R} to signify a 2π rotation, which equals $\mathbb{1}$ and $-\mathbb{1}$ for spinless and spinfull cases respectively.

The two-fold (C_2) and three-fold (C_3) rotation operators transform lattice co-ordinates as follows:

$$\begin{aligned} C_{2x}(x, y, z) &\longrightarrow (x, -y, -z) \\ C_{2y}(x, y, z) &\longrightarrow (-x, y, -z) \\ C_{2z}(x, y, z) &\longrightarrow (-x, -y, z) \\ C_{3,111}(x, y, z) &\longrightarrow (z, x, y) \\ C_{3,111}^{-1}(x, y, z) &\longrightarrow (y, z, x) \end{aligned}$$

The matrix representations of these rotation operators are thus as follows:

$$\begin{aligned} C_{2x} &= \begin{pmatrix} 1 & 0 & 0 \\ 0 & -1 & 0 \\ 0 & 0 & -1 \end{pmatrix}; C_{2y} = \begin{pmatrix} -1 & 0 & 0 \\ 0 & 1 & 0 \\ 0 & 0 & -1 \end{pmatrix} \\ C_{2z} &= \begin{pmatrix} -1 & 0 & 0 \\ 0 & -1 & 0 \\ 0 & 0 & 1 \end{pmatrix}; C_{3,111} = \begin{pmatrix} 0 & 0 & 1 \\ 1 & 0 & 0 \\ 0 & 1 & 0 \end{pmatrix} \end{aligned}$$

and we can use them to multiply rotation operators ($\{\mathcal{O}_1\mathcal{O}_2\mathcal{O}_3\dots\}$) to obtain the net point group operation. Sum of two translation vectors follows the usual rule:

$$(x_1, y_1, z_1) + (x_2, y_2, z_2) \longrightarrow (x_1 + x_2, y_1 + y_2, z_1 + z_2)$$

Furthermore, the color scheme set up above will be used in the remaining text when needed to allow for easy pars-

ing of the various algebraic manipulations. In some algebraic manipulation, any expression with a given color in any line is replaced in the following line by the right hand side of the corresponding colored formula above.

III. SPINLESS

A. Γ point

The little group at Γ point has $S_{2z} = \{C_{2z}|\frac{1}{2}, 0, \frac{1}{2}\}$, $S_{2y} = \{C_{2y}|0, \frac{1}{2}, \frac{1}{2}\}$ & $S_3 = \{C_{3,111}|0, 0, 0\}$ as the symmetry generators.¹⁰ These generators satisfy the following relations:

$$\begin{aligned}
S_{2z}^2 &= \{C_{2z}|\frac{1}{2}, 0, \frac{1}{2}\}\{C_{2z}|\frac{1}{2}, 0, \frac{1}{2}\} \\
&= \{C_{2z}^2|C_{2z}(\frac{1}{2}, 0, \frac{1}{2}) + (\frac{1}{2}, 0, \frac{1}{2})\} \\
&= \{C_{2z}^2|(\frac{\bar{1}}{2}, 0, \frac{1}{2}) + (\frac{1}{2}, 0, \frac{1}{2})\} \\
&= \{C_{2z}^2|0, 0, 1\} \\
&= \{\mathcal{R}|0, 0, 1\} \\
&= \{I|0, 0, 1\} \\
&= 1
\end{aligned} \tag{1}$$

From now onwards, we will skip the derivations of the various relations satisfied by the crystal symmetries, and only focus on the details of the symmetry-protection of the degeneracies. All derivations of crystal symmetry relations are compiled in Sec. VII for reference. Similar to Eq. 1, we also get

$$S_{2y}^2 = 1 \tag{2}$$

$$S_3^3 = 1 \tag{3}$$

The two-fold screws and three-fold rotation $C_{3,111}$ satisfy the following relations:

$$[S_{2z}, S_{2y}] = 0 \tag{4a}$$

$$S_{2z}S_3 = S_3S_{2y} \tag{4b}$$

$$S_3S_{2z}S_{2y} = S_{2y}S_3 \tag{4c}$$

Since S_{2z} and S_{2y} commute, let $|\psi\rangle$ be a simultaneous eigenstate of both S_{2z} and S_{2y} (and also the Hamiltonian since these are the symmetries of the Hamiltonian, i.e. commute with the Hamiltonian by definition). Let

$$\begin{aligned}
S_{2z}|\psi\rangle &= \lambda_1|\psi\rangle \\
S_{2y}|\psi\rangle &= \lambda_2|\psi\rangle
\end{aligned} \tag{5}$$

with $\lambda_1 = \pm 1$, $\lambda_2 = \pm 1$ due to Eqs. 1 and 2.

Using above relations between S_3 , S_{2z} and S_{2y} , we can arrive at

$$S_{2z}S_3|\psi\rangle = S_3S_{2y}|\psi\rangle = \lambda_2S_3|\psi\rangle \tag{6}$$

$$S_{2y}S_3|\psi\rangle = S_3S_{2z}S_{2y}|\psi\rangle = \lambda_1\lambda_2S_3|\psi\rangle$$

$$S_{2z}S_3^2|\psi\rangle = S_3S_{2y}S_3|\psi\rangle = S_3^2S_{2z}S_{2y}|\psi\rangle = \lambda_1\lambda_2S_3^2|\psi\rangle$$

$$S_{2y}S_3^2|\psi\rangle = S_3S_{2z}S_{2y}S_3|\psi\rangle = S_3^2S_{2z}|\psi\rangle = \lambda_1S_3^2|\psi\rangle$$

The set of equations Eqs. (6) show S_3 generates two new distinct eigenstates $S_3|\psi\rangle$ and $S_3^2|\psi\rangle$ of S_{2z} and S_{2y} provided either $\lambda_1 \neq 1$ or $\lambda_2 \neq 1$. In other words, both screws are non-trivial. These three states will be degenerate since S_3 commutes with the Hamiltonian. Thus, these three states ($|\psi\rangle$, $|S_3\psi\rangle$, $|S_3^2\psi\rangle$) together form a three-fold degeneracy at Γ point. The above is a recapitulation of the arguments in Sec. C in Ref. 11's supplementary. The $\lambda_1 = \lambda_2 = 1$ may correspond to a case where both screws are trivial which does not protect any degeneracy, or a case where only one of the screws is trivial which protects only a two-fold degeneracy.

B. R point

The generators at R point are $S_{2x} = \{C_{2x}|\frac{1}{2}, \frac{3}{2}, 0\}$, $S_{2y} = \{C_{2y}|0, \frac{3}{2}, \frac{1}{2}\}$ and $S_3 = \{C_{3,111}^{-1}|0, 1, 0\}$.¹⁰ They satisfy the following:

$$S_{2x}^2 = -1 \tag{7a}$$

$$S_{2y}^2 = -1 \tag{7b}$$

$$S_{2x}S_{2y} = -S_{2y}S_{2x} \tag{7c}$$

$$S_{2x}S_3 = S_3S_{2y} \tag{7d}$$

$$S_3S_{2x}S_{2y} = S_{2y}S_3 \tag{7e}$$

The eigenvalues under the two-fold screws (S_{2x} , S_{2y}) will be unit-modulus and pure imaginary due to Eqs. 7a and 7b. Let $|\psi\rangle$ be an eigenstate of S_{2y} with eigenvalue i without loss of generality, i.e. $S_{2y}|\psi\rangle = i|\psi\rangle$. Then, Eq. 7c implies that $|S_{2x}\psi\rangle \equiv S_{2x}|\psi\rangle$ will be an eigenstate of S_{2y} with eigenvalue $-i$ because

$$S_{2y}|S_{2x}\psi\rangle = S_{2y}S_{2x}|\psi\rangle = -S_{2x}S_{2y}|\psi\rangle = -i|S_{2x}\psi\rangle$$

Since $|\psi\rangle$ and $|S_{2x}\psi\rangle$ have different eigenvalues under S_{2y} , they are orthogonal. Eq. 7d now implies that $|S_3\psi\rangle \equiv S_3|\psi\rangle$ will be an eigenstate of S_{2x} with eigenvalue i because

$$S_{2x}|S_3\psi\rangle = S_{2x}S_3|\psi\rangle = S_3S_{2y}|\psi\rangle = S_3i|\psi\rangle = i|S_3\psi\rangle$$

Eq. 7c will again imply that $|S_{2y}S_3\psi\rangle \equiv S_{2y}S_3|\psi\rangle$ will be an eigenstate of S_{2x} with eigenvalue $-i$ because

$$S_{2x}|S_{2y}S_3\psi\rangle = S_{2x}S_{2y}|S_3\psi\rangle = -S_{2y}S_{2x}|S_3\psi\rangle = -i|S_{2y}S_3\psi\rangle$$

Since $|S_3\psi\rangle$ and $|S_{2y}S_3\psi\rangle$ have different eigenvalues under S_{2x} , they are orthogonal.¹²

By requiring that S_3 acts non-trivially on the eigenstates of S_{2y} and takes out of the subspace formed by them, we can ensure mutual orthogonality between eigenstates of S_{2y} and S_{2x} . Minimally, $\langle\psi|S_3|\psi\rangle = 0$ guarantees all other mutual orthogonalities as follows:

Case of $|S_3\psi\rangle$ and $|S_{2x}\psi\rangle$:

$$\begin{aligned}\langle S_{2x}\psi|S_3\psi\rangle &= \langle\psi|S_{2x}^{-1}S_3|\psi\rangle = \langle\psi|(-S_{2x})S_3|\psi\rangle \\ &= -\langle\psi|S_{2x}S_3|\psi\rangle = \langle\psi|S_3S_{2y}|\psi\rangle \\ &= i\langle\psi|S_3|\psi\rangle = 0.\end{aligned}$$

Case of $|S_{2y}S_3\psi\rangle$ and $|\psi\rangle$:

$$\begin{aligned}\langle\psi|S_{2y}S_3\psi\rangle &= \langle\psi|S_{2y}S_3|\psi\rangle = -\langle\psi|S_{2y}^{-1}S_3|\psi\rangle \\ &= -(-i)\langle\psi|S_3|\psi\rangle = 0\end{aligned}$$

Case of $|S_{2y}S_3\psi\rangle$ and $|S_{2x}\psi\rangle$:

$$\begin{aligned}\langle S_{2x}\psi|S_{2y}S_3\psi\rangle &= \langle\psi|S_{2x}^{-1}S_{2y}S_3|\psi\rangle \\ &= \langle\psi|(-S_{2x})S_{2y}S_3|\psi\rangle \\ &= -\langle\psi|S_{2x}|S_{2y}S_3\psi\rangle \\ &= i\langle\psi|S_{2y}S_3\psi\rangle = 0\end{aligned}$$

Therefore, $(|\psi\rangle, |S_{2x}\psi\rangle, |S_3\psi\rangle, |S_{2y}S_3\psi\rangle)$ are four mutually orthogonal states. Thus, we have a symmetry-protected four-fold degeneracy at R point in the absence of spin-orbit coupling.

Since time-reversal squares to identity ($\mathcal{T}^2 = \mathbb{1}$) for spinless fermions, it does not generate any new eigenstates. In fact, it relates the eigenstates of the two screws as follows:

$$\begin{aligned}S_{2y}|\mathcal{T}\psi\rangle &= S_{2y}\mathcal{T}|\psi\rangle = \mathcal{T}S_{2y}|\psi\rangle = \mathcal{T}i|\psi\rangle = -i\mathcal{T}|\psi\rangle \\ \Rightarrow S_{2y}|\mathcal{T}\psi\rangle &= -i|\mathcal{T}\psi\rangle\end{aligned}$$

where we have used the facts that \mathcal{T} commutes with the screws, and $\mathcal{T}^\dagger i\mathcal{T} = -i$ (anti-linear property). Thus, we can identify $|\mathcal{T}\psi\rangle$ with $|S_{2x}\psi\rangle$ having same eigenvalue $-i$ under S_{2y} . By a very similar argument, the pairs $\{|\mathcal{T}S_{2x}\psi\rangle, |\psi\rangle\}$, $\{|\mathcal{T}S_3\psi\rangle, |S_{2y}S_3\psi\rangle\}$ and $\{|\mathcal{T}S_{2y}S_3\psi\rangle, |S_3|\psi\rangle\}$ can be identified.

C. Four-fold degeneracy at R point for spinless case in few other binary and ternary systems of space group 198

In addition to CoGe in main article, here in Fig. 1, we showcase the band structures of few other binary and also ternary systems of space group 198 in the absence of spin-orbit coupling. Similar to CoGe, the electronic structure in all these binary and ternary systems shows the four-fold degeneracy at R point irrespective of their location with respect to Fermi level. Thus, the four-fold degeneracy at R point for the spinless case is independent of both the chemical elements at the lattice sites and number of atoms in the cell. Rather, the degeneracy at R point is strictly determined by the crystal space group symmetry.

IV. SPINFULL

The generators at Γ point are $S_{2z} = \{C_{2z}|\frac{1}{2}, 0, \frac{1}{2}\}$, $S_{2y} = \{C_{2y}|0, \frac{1}{2}, \frac{1}{2}\}$ & $S_3 = \{C_{3,111}|0, 0, 0\}$.¹⁰ They satisfying the following relations for spinfull fermions:

$$S_{2z}^2 = -1 \quad (8a)$$

$$S_{2y}^2 = -1 \quad (8b)$$

$$S_3^3 = -1 \quad (8c)$$

The difference with respect to the corresponding spinless Γ point symmetry relations is due to the different action of \mathcal{R} in these two cases.

Also, we have

$$S_{2z}S_{2y} = -S_{2y}S_{2z} \quad (9a)$$

$$S_{2z}S_3 = S_3S_{2y} \quad (9b)$$

$$S_3S_{2z}S_{2y} = S_{2y}S_3 \quad (9c)$$

Therefore, we can use the very same arguments as in Sec. IIIB to generate a four-fold degeneracy.

Since $\mathcal{T}^2 = -1$ for the spinfull case, so it is possible that time reversal may generate further new states. In other words, the question is whether the time-reversed partners of the above four-fold states $\{|\psi\rangle, |S_{2z}\psi\rangle, |S_3\psi\rangle, |S_{2y}S_3\psi\rangle\}$ are distinctly new states or not? As mentioned in the main text, they are actually not new states because mutual orthogonalities are not ensured. This is due to the imaginary eigenvalues under screws.

From $S_{2z}^2 = S_{2y}^2 = \mathcal{T}^2 = -1$, we have $S_{2z}^{-1} = -S_{2z}$, $S_{2y}^{-1} = -S_{2y}$ and $\mathcal{T}^{-1} = -\mathcal{T}$. Also \mathcal{T} commutes with the screws. Firstly, these mutual overlaps have to be real. E.g.

$$\begin{aligned}\langle S_{2z}\psi|\mathcal{T}\psi\rangle &= \langle\psi|S_{2z}^{-1}\mathcal{T}|\psi\rangle = -\langle\psi|S_{2z}\mathcal{T}|\psi\rangle = -\langle\psi|\mathcal{T}S_{2z}|\psi\rangle \\ &= \langle\psi|\mathcal{T}^{-1}S_{2z}|\psi\rangle = \langle\mathcal{T}\psi|S_{2z}\psi\rangle = \langle S_{2z}\psi|\mathcal{T}\psi\rangle^*\end{aligned}$$

Secondly, the eigenvalue of $|\mathcal{T}\psi\rangle$ under S_{2y} is same as $|S_{2z}\psi\rangle$, and similarly the eigenvalue of $|\mathcal{T}S_{2z}\psi\rangle$ under S_{2y} is same as $|\psi\rangle$ as follows: Let, $S_{2y}|\psi\rangle = i|\psi\rangle$ Therefore,

$$S_{2y}|S_{2z}\psi\rangle = -i|S_{2z}\psi\rangle$$

by following the same argument as in Sec. IIIB. Now,

$$\begin{aligned}S_{2y}|\mathcal{T}\psi\rangle &= S_{2y}\mathcal{T}|\psi\rangle = \mathcal{T}S_{2y}|\psi\rangle = \mathcal{T}i|\psi\rangle \\ &= -i\mathcal{T}|\psi\rangle = -i|\mathcal{T}\psi\rangle.\end{aligned}$$

Thus, both $|\mathcal{T}\psi\rangle$ and $|S_{2z}\psi\rangle$ have the same eigenvalues under S_{2y} , and we can not conclude anything about this mutual orthogonality. The same lack of mutual orthogonality will be the case for

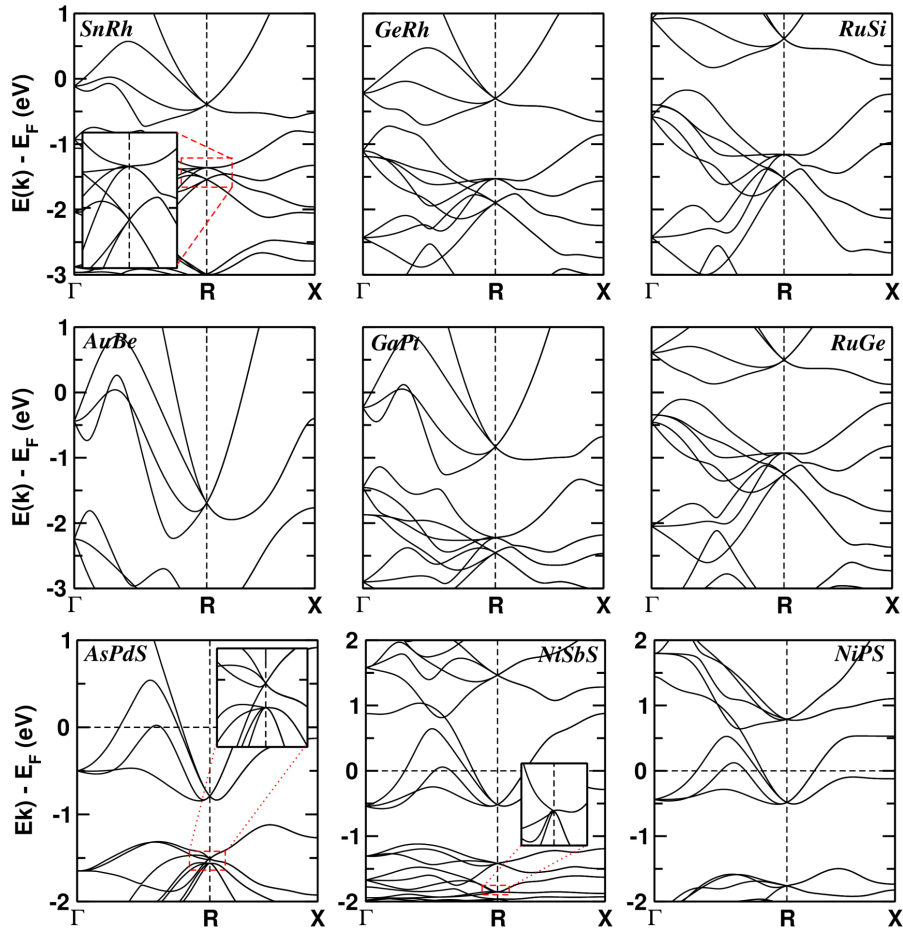


FIG. 1. (Color online) Band structure for few others binary and ternary systems of space group 198. The inset in the figures are enlarged view of closely spaced four-fold degenerate nodes.

the other pairs $\{|\psi\rangle, |\mathcal{T}S_{2z}\psi\rangle\}$, $\{|S_3\psi\rangle, |\mathcal{T}S_{2y}S_3\psi\rangle\}$ and $\{|S_{2y}S_3\psi\rangle, |\mathcal{T}S_3\psi\rangle\}$. Thus, we can at most get a four-fold degeneracy ($\{|\psi\rangle, |S_{2z}\psi\rangle, |S_3\psi\rangle, |S_{2y}S_3\psi\rangle\}$) at Γ point for spinfull fermions in SG 198.

We also note here that for R point, since now the screws commute and square to 1, the eigenvalues are unit modulus and purely real. We can get a three-fold degeneracy ($\{|\psi\rangle, |S_3\psi\rangle, |S_3^2\psi\rangle\}$) by following the same arguments as in Sec. III A. Furthermore due to eigenvalues being real, the above mutual orthogonalities under time reversal are ensured, and we have three distinctly new time-reversed partners ($\{|\mathcal{T}\psi\rangle, |\mathcal{T}S_3\psi\rangle, |\mathcal{T}S_3^2\psi\rangle\}$). This can give a symmetry-protected six-fold degeneracy at R spinfull case as discussed in Ref. 11.

V. TWO FOLD DEGENERACIES ALONG R-X AND M-X DIRECTION

A. Spinless

The screw rotation along x -axis is $S_{2x} = \{C_{2x}|\frac{1}{2}, \frac{1}{2}, 0\}$. We can define an anti-unitary operator $\Theta_{2x} = \mathcal{T}S_{2x}$. \mathcal{T} squares to +1 for spinless case, and commutes with the (unitary) screw. Thus we have

$$\begin{aligned}
 \Theta_{2x}^2 &= \mathcal{T}S_{2x}\mathcal{T}S_{2x} \\
 &= \mathcal{T}^2 S_{2x}^2 \\
 &= \mathcal{T}^2 \{C_{2x}|\frac{1}{2}, \frac{1}{2}, 0\} \{C_{2x}|\frac{1}{2}, \frac{1}{2}, 0\} \\
 &= \mathcal{T}^2 \{C_{2x}^2 | C_{2x} \left(\frac{1}{2}, \frac{1}{2}, 0\right) + \left(\frac{1}{2}, \frac{1}{2}, 0\right)\} \\
 &= \mathcal{T}^2 \{C_{2x}^2 | \left(\frac{1}{2}, \bar{1}, 0\right) + \left(\frac{1}{2}, \frac{1}{2}, 0\right)\}
 \end{aligned}$$

$$\begin{aligned}
&= \mathcal{T}^2\{C_{2x}^2|1, 0, 0\} \\
&= \mathcal{T}^2\{\mathcal{R}|1, 0, 0\} \\
&= \{\mathcal{R}|1, 0, 0\} \\
&= \{\mathbb{1}|1, 0, 0\} \\
&= e^{-ik_x}
\end{aligned} \tag{10}$$

Therefore, on the $k_x = \pi$ plane, $\Theta_{2x}^2 = -1$. Thus, by Kramer's argument, if $|\psi\rangle$ is an eigenstate of S_{2x} , then $|\Theta_{2x}\psi\rangle$ is like a time-reversed partner for $k_x = \pi$. Hence, Θ_{2x} gives a Kramer's like double degeneracy on the $k_x = \pi$ and symmetry-related planes. This in turn implies that the bands along R-X and M-X directions in the Brillouin zone are two-fold degenerate by the combination of time-reversal and screw symmetry as seen in Fig. 2 of the main text.

B. Spinfull

For spinfull case, $\mathcal{R} = -\mathbb{1}$ and $\mathcal{T}^2 = -\mathbb{1}$. Therefore, similar to Eq. (10), it follows that

$$\begin{aligned}
\Theta_{2x}^2 &= \mathcal{T}S_{2x}\mathcal{T}S_{2x} \\
&= \mathcal{T}^2S_{2x}^2 \\
&= \mathcal{T}^2\{C_{2x}^2|1, 0, 0\} \\
&= \mathcal{T}^2\{\mathcal{R}|1, 0, 0\} \\
&= -\mathbb{1}\{-\mathbb{1}|1, 0, 0\} \\
&= +e^{-ik_x}
\end{aligned}$$

Thus, similar to the spinless case, $\Theta_{2x}^2 = -1$ again and the bands are doubly degenerate on $k_x = \pi$ and symmetry-related planes even in the spinfull case. These gives the double degeneracy of bands along R-X and M-X and symmetry-related directions in the Brillouin zone as also observed in Fig. 3 of the main text. We note here that this is again a Kramer's-like degeneracy ensured by a combination of time reversal and screw symmetry on these planes, and not the standard Kramer's degeneracy which can not be applied here since inversion symmetry is absent. Screw symmetry is replacing the inversion symmetry on these high-symmetry planes to again make the Kramer's argument operational and give us a Kramer's-like two-fold degeneracy.

VI. ELECTRONIC STRUCTURE FOR COGE FOR SPACE GROUP $C2/m$

As mentioned in the main text, CoGe requires high pressure to crystallize in SG 198 ($P2_13$).¹³ However, at ambient pressure it crystallize in the SG 12 ($C2/m$).¹⁴ All of the symmetry-protection of SG 198 are not expected for SG 12. Figure 2 shows the electronic structure of

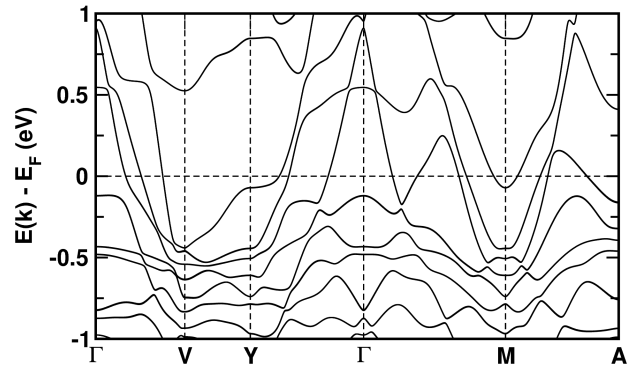


FIG. 2. (Color online) Band structure along high symmetry directions for CoGe crystallizes in space group $C2/m$.

CoGe crystal in space group $C2/m$. Indeed, the band structure clearly shows the absence of the multi-fold band degeneracies at time reversal invariant momenta (Γ and R).

VII. COMPENDIUM OF SYMMETRY RELATIONS

We recall the various formulas that will be used below.

$$\begin{aligned}
\{\mathcal{O}_1|\vec{t}_1\}\{\mathcal{O}_2|\vec{t}_2\} &= \{\mathcal{O}_1\mathcal{O}_2|\mathcal{O}_1\vec{t}_2 + \vec{t}_1\} \\
\{\mathcal{O}|\vec{t}\}^{-1} &= \{\mathcal{O}^{-1}|-\mathcal{O}^{-1}\vec{t}\} \\
\{\mathbb{1}|\vec{t}\} &= e^{-i\vec{k}\cdot\vec{t}} \\
C_{2x}(x, y, z) &\longrightarrow (x, -y, -z) \\
C_{2y}(x, y, z) &\longrightarrow (-x, y, -z) \\
C_{2z}(x, y, z) &\longrightarrow (-x, -y, z) \\
C_{3,111}(x, y, z) &\longrightarrow (z, x, y) \\
C_{3,111}^{-1}(x, y, z) &\longrightarrow (y, z, x) \\
(x_1, y_1, z_1) + (x_2, y_2, z_2) &\longrightarrow (x_1 + x_2, y_1 + y_2, z_1 + z_2)
\end{aligned}$$

From the first relation, it also follows that

$$\begin{aligned}
\{\mathcal{O}_1\mathcal{O}_2|x, y, z\} &= \{\mathcal{O}_1|p, q, r\}\{\mathcal{O}_2|l, m, n\}\{\mathbb{1}|a, b, c\} \\
\{\mathcal{O}|\vec{u}, \vec{v}, \vec{w}\} &= \{\mathcal{O}|u, v, w\}\{\mathbb{1}|\alpha, \beta, \gamma\}
\end{aligned}$$

where $(x, y, z) = \mathcal{O}_1(\mathcal{O}_2(a, b, c) + (l, m, n)) + (p, q, r)$, $(\vec{u}, \vec{v}, \vec{w}) = \mathcal{O}(\alpha, \beta, \gamma) + (u, v, w)$ and $\mathbb{1}$ is identity. This relation is also useful in some of the derivations.

Eq. (2) ($S_{2y}^2 = 1$):–

$$\begin{aligned}
&S_{2y}^2 \\
&= \{C_{2y}|0, \frac{1}{2}, \frac{1}{2}\}\{C_{2y}|0, \frac{1}{2}, \frac{1}{2}\} \\
&= \{C_{2y}^2|C_{2y}\left(0, \frac{1}{2}, \frac{1}{2}\right) + \left(0, \frac{1}{2}, \frac{1}{2}\right)\} \\
&= \{C_{2y}^2|\left(0, \frac{1}{2}, \frac{1}{2}\right) + \left(0, \frac{1}{2}, \frac{1}{2}\right)\} \\
&= \{C_{2y}^2|0, 1, 0\} \\
&= \{\mathcal{R}|0, 1, 0\} \\
&= \{\mathbb{1}|0, 1, 0\} \\
&= 1 \\
&\Rightarrow S_{2y}^2 = 1
\end{aligned}$$

Eq. (3) ($S_3^3 = 1$):–

$$\begin{aligned}
&S_3^3 \\
&= \{C_{3,111}|0, 0, 0\}^3 = \{C_{3,111}^3|0, 0, 0\} \\
&= \{\mathcal{R}|0, 0, 0\} \\
&= \{\mathbb{1}|0, 0, 0\} \\
&= 1 \\
&\Rightarrow S_3^3 = 1
\end{aligned}$$

Eq. (4a) ($[\mathbf{S}_{2z}, \mathbf{S}_{2y}] = \mathbf{0}$):-

$$\begin{aligned}
& S_{2z}S_{2y} \\
&= \{C_{2z}|\frac{1}{2}, 0, \frac{1}{2}\}\{C_{2y}|0, \frac{1}{2}, \frac{1}{2}\} \\
&= \{C_{2z}C_{2y}|C_{2z}\left(0, \frac{1}{2}, \frac{1}{2}\right) + \left(\frac{1}{2}, 0, \frac{1}{2}\right)\} \\
&= \{C_{2z}C_{2y}|\frac{1}{2}, \bar{1}, 1\} \\
&= \{\mathcal{R}C_{2y}C_{2z}|\frac{1}{2}, \bar{1}, 1\} \\
&= \{\mathbb{1}C_{2y}C_{2z}|\frac{1}{2}, \bar{1}, 1\} \\
&= \{C_{2y}C_{2z}|\frac{1}{2}, \bar{1}, 1\} \\
&= \{C_{2y}|0, \frac{1}{2}, \frac{1}{2}\}\{C_{2z}|\frac{1}{2}, 0, \frac{1}{2}\}\{\mathbb{1}|1, 1, \bar{1}\} \\
&= S_{2y}S_{2z}\{\mathbb{1}|1, 1, \bar{1}\} \\
&= S_{2y}S_{2z} \\
&\Rightarrow [S_{2z}, S_{2y}] = 0
\end{aligned}$$

Eq. (4b) ($\mathbf{S}_{2z}\mathbf{S}_3 = \mathbf{S}_3\mathbf{S}_{2y}$):-

$$\begin{aligned}
& S_3^{-1}S_{2z}S_3 \\
&= \{C_{3,111}|0, 0, 0\}^{-1}\{C_{2z}|\frac{1}{2}, 0, \frac{1}{2}\}\{C_{3,111}|0, 0, 0\} \\
&= \{C_{3,111}^{-1}|0, 0, 0\}\{C_{2z}|\frac{1}{2}, 0, \frac{1}{2}\}\{C_{3,111}|0, 0, 0\} \\
&= \{C_{3,111}^{-1}|0, 0, 0\}\{C_{2z}C_{3,111}|\frac{1}{2}, 0, \frac{1}{2}\} \\
&= \{C_{3,111}^{-1}C_{2z}C_{3,111}|C_{3,111}^{-1}\left(\frac{1}{2}, 0, \frac{1}{2}\right)\} \\
&= \{C_{2y}|C_{3,111}^{-1}\left(\frac{1}{2}, 0, \frac{1}{2}\right)\} \\
&= \{C_{2y}|0, \frac{1}{2}, \frac{1}{2}\} \\
&= S_{2y} \\
&\Rightarrow S_{2z}S_3 = S_3S_{2y}
\end{aligned}$$

Eq. (4c) ($\mathbf{S}_3\mathbf{S}_{2z}\mathbf{S}_{2y} = \mathbf{S}_{2y}\mathbf{S}_3$):-

$$\begin{aligned}
& S_3 S_{2z} S_{2y} S_3^{-1} \\
&= \{C_{3,111}|0,0,0\}\{C_{2z}|\frac{1}{2},0,\frac{1}{2}\}\{C_{2y}|0,\frac{1}{2},\frac{1}{2}\}\{C_{3,111}|0,0,0\}^{-1} \\
&= \{C_{3,111}|0,0,0\}\{C_{2z}C_{2y}|\frac{1}{2},\frac{1}{2},1\}\{C_{3,111}|0,0,0\}^{-1} \\
&= \{C_{3,111}C_{2z}C_{2y}|1,\frac{1}{2},\frac{1}{2}\}\{C_{3,111}|0,0,0\}^{-1} \\
&= \{C_{3,111}C_{2z}C_{2y}|1,\frac{1}{2},\frac{1}{2}\}\{C_{3,111}^{-1}|0,0,0\} \\
&= \{C_{3,111}C_{2z}C_{2y}C_{3,111}^{-1}|1,\frac{1}{2},\frac{1}{2}\} \\
&= \{C_{2y}|1,\frac{1}{2},\frac{1}{2}\} \\
&= \{C_{2y}|0,\frac{1}{2},\frac{1}{2}\}\{0|\bar{1},0,1\} \\
&= S_{2y} \\
&\Rightarrow S_3 S_{2z} S_{2y} = S_{2y} S_3
\end{aligned}$$

Eq. (7a) ($\mathbf{S}_{2x}^2 = -1$):-

$$\begin{aligned}
& S_{2x}^2 \\
&= \{C_{2x}|\frac{1}{2},\frac{3}{2},0\}\{C_{2x}|\frac{1}{2},\frac{3}{2},0\} \\
&= \{C_{2x}^2|C_{2x}\left(\frac{1}{2},\frac{3}{2},0\right) + \left(\frac{1}{2},\frac{3}{2},0\right)\} \\
&= \{C_{2x}^2|\left(\frac{1}{2},\frac{3}{2},0\right) + \left(\frac{1}{2},\frac{3}{2},0\right)\} \\
&= \{C_{2x}^2|1,0,0\} \\
&= \{\mathcal{R}|1,0,0\} \\
&= \{0|1,0,0\} \\
&= e^{-i\pi} \\
&= -1 \\
&\Rightarrow S_{2x}^2 = -1
\end{aligned}$$

Eq. (7b) ($\mathbf{S}_{2y}^2 = -1$):-

$$\begin{aligned}
& S_{2y}^2 \\
&= \{C_{2y}|0,\frac{3}{2},\frac{1}{2}\}\{C_{2y}|0,\frac{3}{2},\frac{1}{2}\} \\
&= \{C_{2y}^2|C_{2y}\left(0,\frac{3}{2},\frac{1}{2}\right) + \left(0,\frac{3}{2},\frac{1}{2}\right)\} \\
&= \{C_{2y}^2|\left(0,\frac{3}{2},\frac{1}{2}\right) + \left(0,\frac{3}{2},\frac{1}{2}\right)\} \\
&= \{C_{2y}^2|0,3,0\} \\
&= \{\mathcal{R}|0,3,0\} \\
&= \{0|0,3,0\} \\
&= e^{-3i\pi} \\
&= -1 \\
&\Rightarrow S_{2y}^2 = -1
\end{aligned}$$

Eq. (7c) ($\mathbf{S}_{2x}\mathbf{S}_{2y} = -\mathbf{S}_{2y}\mathbf{S}_{2x}$):-

$$\begin{aligned}
& S_{2x}S_{2y} \\
&= \{C_{2x}|\frac{1}{2}, \frac{3}{2}, 0\}\{C_{2y}|0, \frac{3}{2}, \frac{1}{2}\} \\
&= \{C_{2x}C_{2y}|\frac{1}{2}, 0, \frac{\bar{1}}{2}\} \\
&= \{\mathcal{R}C_{2y}C_{2x}|\frac{1}{2}, 0, \frac{\bar{1}}{2}\} \\
&= \{\mathbb{I}C_{2y}C_{2x}|\frac{1}{2}, 0, \frac{\bar{1}}{2}\} \\
&= \{C_{2y}C_{2x}|\frac{1}{2}, 0, \frac{\bar{1}}{2}\} \\
&= \{C_{2y}|0, \frac{3}{2}, \frac{1}{2}\}\{C_{2x}|\frac{1}{2}, \frac{3}{2}, 0\}\{\mathbb{I}|\bar{1}, 3, \bar{1}\} \\
&= S_{2y}S_{2x}\{\mathbb{I}|\bar{1}, 3, \bar{1}\} \\
&= S_{2y}S_{2x}e^{-i(-\pi+3\pi-\pi)} \\
&= -S_{2y}S_{2x} \\
&\Rightarrow S_{2x}S_{2y} = -S_{2y}S_{2x}
\end{aligned}$$

Eq. (7d) ($\mathbf{S}_{2x}\mathbf{S}_3 = \mathbf{S}_3\mathbf{S}_{2y}$):-

$$\begin{aligned}
& S_3^{-1}S_{2x}S_3 \\
&= \{C_{3,111}^{-1}|0, 1, 0\}^{-1}\{C_{2x}|\frac{1}{2}, \frac{3}{2}, 0\}\{C_{3,111}^{-1}|0, 1, 0\} \\
&= \{C_{3,111}| -C_{3,111}(0, 1, 0)\}\{C_{2x}|\frac{1}{2}, \frac{3}{2}, 0\}\{C_{3,111}^{-1}|0, 1, 0\} \\
&= \{C_{3,111}|0, 0, -1\}\{C_{2x}|\frac{1}{2}, \frac{3}{2}, 0\}\{C_{3,111}^{-1}|0, 1, 0\} \\
&= \{C_{3,111}C_{2x}|C_{3,111}\left(\frac{1}{2}, \frac{3}{2}, 0\right) + (0, 0, -1)\}\{C_{3,111}^{-1}|0, 1, 0\} \\
&= \{C_{3,111}C_{2x}|\left(0, \frac{1}{2}, \frac{3}{2}\right) + (0, 0, -1)\}\{C_{3,111}^{-1}|0, 1, 0\} \\
&= \{C_{3,111}C_{2x}|0, \frac{1}{2}, \frac{1}{2}\}\{C_{3,111}^{-1}|0, 1, 0\} \\
&= \{C_{3,111}C_{2x}C_{3,111}^{-1}|C_{3,111}C_{2x}(0, 1, 0) + \left(0, \frac{1}{2}, \frac{1}{2}\right)\} \\
&= \{C_{3,111}C_{2x}C_{3,111}^{-1}|(0, 0, \bar{1}) + \left(0, \frac{1}{2}, \frac{1}{2}\right)\} \\
&= \{C_{3,111}C_{2x}C_{3,111}^{-1}|0, \frac{1}{2}, \frac{\bar{1}}{2}\} \\
&= \{C_{2y}|0, \frac{3}{2}, \frac{1}{2}\}\{\mathbb{I}|0, \bar{1}, 1\} \\
&= \{C_{2y}|0, \frac{3}{2}, \frac{1}{2}\}e^{-i(-\pi+\pi)} \\
&= S_{2y} \\
&\Rightarrow S_{2x}S_3 = S_3S_{2y}
\end{aligned}$$

Eq. (7e) ($\mathbf{S}_3\mathbf{S}_{2x}\mathbf{S}_{2y} = \mathbf{S}_{2y}\mathbf{S}_3$):-

$$\begin{aligned}
& S_3 S_{2x} S_{2y} S_3^{-1} \\
&= \{C_{3,111}^{-1}|0, 1, 0\} \{C_{2x}|\frac{1}{2}, \frac{3}{2}, 0\} \{C_{2y}|0, \frac{3}{2}, \frac{1}{2}\} \\
&\quad \{C_{3,111}^{-1}|0, 1, 0\}^{-1} \\
&= \{C_{3,111}^{-1}|0, 1, 0\} \{C_{2x}C_{2y}|\frac{1}{2}, 0, \bar{1}\} \{C_{3,111}^{-1}|0, 1, 0\}^{-1} \\
&= \{C_{3,111}^{-1}C_{2x}C_{2y}|C_{3,111}^{-1}\left(\frac{1}{2}, 0, \bar{1}\right) + (0, 1, 0)\} \\
&\quad \{C_{3,111}^{-1}|0, 1, 0\}^{-1} \\
&= \{C_{3,111}^{-1}C_{2x}C_{2y}|0, \frac{1}{2}, \frac{1}{2}\} \{C_{3,111}| - C_{3,111}(0, 1, 0)\} \\
&= \{C_{3,111}^{-1}C_{2x}C_{2y}|0, \frac{1}{2}, \frac{1}{2}\} \{C_{3,111}|0, 0, \bar{1}\} \\
&= \{C_{3,111}^{-1}C_{2x}C_{2y}C_{3,111}|C_{3,111}^{-1}C_{2x}C_{2y}(0, 0, \bar{1}) + \left(0, \frac{1}{2}, \frac{1}{2}\right)\} \\
&= \{C_{3,111}^{-1}C_{2x}C_{2y}C_{3,111}|(0, \bar{1}, 0) + \left(0, \frac{1}{2}, \frac{1}{2}\right)\} \\
&= \{C_{3,111}^{-1}C_{2x}C_{2y}C_{3,111}|0, \frac{\bar{1}}{2}, \frac{1}{2}\} \\
&= \{C_{2y}|0, \frac{\bar{1}}{2}, \frac{1}{2}\} \\
&= \{C_{2y}|0, \frac{3}{2}, \frac{1}{2}\} \{||0, \bar{2}, 0\} \\
&= S_{2y} \\
&\Rightarrow S_3 S_{2x} S_{2y} = S_{2y} S_3
\end{aligned}$$

Eq. (8a) ($\mathbf{S}_{2z}^2 = -1$):-

$$\begin{aligned}
& S_{2z}^2 \\
&= \{C_{2z}|\frac{1}{2}, 0, \frac{1}{2}\} \{C_{2z}|\frac{1}{2}, 0, \frac{1}{2}\} \\
&= \{C_{2z}^2|C_{2z}\left(\frac{1}{2}, 0, \frac{1}{2}\right) + \left(\frac{1}{2}, 0, \frac{1}{2}\right)\} \\
&= \{C_{2z}^2|\left(\frac{\bar{1}}{2}, 0, \frac{1}{2}\right) + \left(\frac{1}{2}, 0, \frac{1}{2}\right)\} \\
&= \{C_{2z}^2|0, 0, 1\} \\
&= \{\mathcal{R}|0, 0, 1\} \\
&= -\{||0, 0, 1\} \\
&= -1
\end{aligned}$$

Eq. (8b) ($S_{2y}^2 = -1$):-

$$\begin{aligned}
& S_{2y}^2 \\
&= \{C_{2y}|0, \frac{1}{2}, \frac{1}{2}\}\{C_{2y}|0, \frac{1}{2}, \frac{1}{2}\} \\
&= \{C_{2y}^2|C_{2y}\left(0, \frac{1}{2}, \frac{1}{2}\right) + \left(0, \frac{1}{2}, \frac{1}{2}\right)\} \\
&= \{C_{2y}^2|\left(0, \frac{1}{2}, \bar{\frac{1}{2}}\right) + \left(0, \frac{1}{2}, \frac{1}{2}\right)\} \\
&= \{C_{2y}^2|0, 1, 0\} \\
&= \{\mathcal{R}|0, 1, 0\} \\
&= -\{\mathbb{I}|0, 1, 0\} \\
&= -1
\end{aligned}$$

Eq. (8c) ($S_3^3 = -1$):-

$$\begin{aligned}
& S_3^3 \\
&= \{C_{3,111}|0, 0, 0\}^3 = \{C_{3,111}^3|0, 0, 0\} \\
&= \{\mathcal{R}|0, 0, 0\} \\
&= -\{\mathbb{I}|0, 0, 0\} \\
&= -1 \\
&\Rightarrow S_3^3 = -1
\end{aligned}$$

Eq. (9a) ($S_{2z}S_{2y} = -S_{2y}S_{2z}$):-

$$\begin{aligned}
& S_{2z}S_{2y} \\
&= \{C_{2z}|\frac{1}{2}, 0, \frac{1}{2}\}\{C_{2y}|0, \frac{1}{2}, \frac{1}{2}\} \\
&= \{C_{2z}C_{2y}|C_{2z}\left(0, \frac{1}{2}, \frac{1}{2}\right) + \left(\frac{1}{2}, 0, \frac{1}{2}\right)\} \\
&= \{C_{2z}C_{2y}|\frac{1}{2}, \bar{\frac{1}{2}}, 1\} \\
&= \{\mathcal{R}C_{2y}C_{2z}|\frac{1}{2}, \bar{\frac{1}{2}}, 1\} \\
&= \{-\mathbb{I}C_{2y}C_{2z}|\frac{1}{2}, \bar{\frac{1}{2}}, 1\} \\
&= -\{C_{2y}C_{2z}|\frac{1}{2}, \bar{\frac{1}{2}}, 1\} \\
&= -\{C_{2y}|0, \frac{1}{2}, \frac{1}{2}\}\{C_{2z}|\frac{1}{2}, 0, \frac{1}{2}\}\{\mathbb{I}|1, 1, \bar{1}\} \\
&= -S_{2y}S_{2z} \\
&\Rightarrow S_{2z}S_{2y} = -S_{2y}S_{2z}
\end{aligned}$$

Eq. (9b) ($\mathbf{S}_{2z}\mathbf{S}_3 = \mathbf{S}_3\mathbf{S}_{2y}$):-

$$\begin{aligned}
& S_3^{-1}S_{2z}S_3 \\
&= \{C_{3,111}|0,0,0\}^{-1}\{C_{2z}|\frac{1}{2},0,\frac{1}{2}\}\{C_{3,111}|0,0,0\} \\
&= \{C_{3,111}|0,0,0\}^{-1}\{C_{2z}C_{3,111}|\frac{1}{2},0,\frac{1}{2}\} \\
&= \{C_{3,111}^{-1}|0,0,0\}\{C_{2z}C_{3,111}|\frac{1}{2},0,\frac{1}{2}\} \\
&= \{C_{3,111}^{-1}C_{2z}C_{3,111}|C_{3,111}^{-1}\left(\frac{1}{2},0,\frac{1}{2}\right) + (0,0,0)\} \\
&= \{C_{3,111}^{-1}C_{2z}C_{3,111}|0,\frac{1}{2},\frac{1}{2}\} \\
&= \{C_{2y}|0,\frac{1}{2},\frac{1}{2}\} \\
&= S_{2y} \\
&\Rightarrow S_{2z}S_3 = S_3S_{2y}
\end{aligned}$$

Eq. (9c) ($\mathbf{S}_3\mathbf{S}_{2z}\mathbf{S}_{2y} = \mathbf{S}_{2y}\mathbf{S}_3$):-

$$\begin{aligned}
& S_3S_{2z}S_{2y}S_3^{-1} \\
&= \{C_{3,111}|0,0,0\}\{C_{2z}|\frac{1}{2},0,\frac{1}{2}\}\{C_{2y}|0,\frac{1}{2},\frac{1}{2}\} \\
&\quad \{C_{3,111}|0,0,0\}^{-1} \\
&= \{C_{3,111}|0,0,0\}\{C_{2z}C_{2y}|C_{2z}\left(0,\frac{1}{2},\frac{1}{2}\right) + \left(\frac{1}{2},0,\frac{1}{2}\right)\} \\
&\quad \{C_{3,111}|0,0,0\}^{-1} \\
&= \{C_{3,111}|0,0,0\}\{C_{2z}C_{2y}|\left(0,\frac{\bar{1}}{2},\frac{1}{2}\right) + \left(\frac{1}{2},0,\frac{1}{2}\right)\} \\
&\quad \{C_{3,111}|0,0,0\}^{-1} \\
&= \{C_{3,111}|0,0,0\}\{C_{2z}C_{2y}|\frac{1}{2},\frac{\bar{1}}{2},1\}\{C_{3,111}|0,0,0\}^{-1} \\
&= \{C_{3,111}C_{2z}C_{2y}|C_{3,111}\left(\frac{1}{2},\frac{\bar{1}}{2},1\right)\}\{C_{3,111}|0,0,0\}^{-1} \\
&= \{C_{3,111}C_{2z}C_{2y}|1,\frac{1}{2},\frac{\bar{1}}{2}\}\{C_{3,111}|0,0,0\}^{-1} \\
&= \{C_{3,111}C_{2z}C_{2y}|1,\frac{1}{2},\frac{\bar{1}}{2}\}\{C_{3,111}^{-1}|0,0,0\} \\
&= \{C_{3,111}C_{2z}C_{2y}C_{3,111}^{-1}|1,\frac{1}{2},\frac{\bar{1}}{2}\} \\
&= \{C_{2y}|1,\frac{1}{2},\frac{\bar{1}}{2}\} \\
&= \{C_{2y}|0,\frac{1}{2},\frac{1}{2}\}\{0|\bar{1},0,1\} \\
&= S_{2y} \\
&\Rightarrow S_3S_{2z}S_{2y} = S_{2y}S_3
\end{aligned}$$

* These two authors have contributed equally to this work

† biswarup@iiti.ac.in

‡ aftar@iitb.ac.in

- ¹ P. E. Böchl, Phys. Rev. B **50**, 17953 (1994).
- ² Nicola Marzari and David Vanderbilt, Phys. Rev. B **56**,12847 (1997).
- ³ Ivo Souza, Nicola Marzari, and David Vanderbilt, Phys. Rev. B **65**, 035109 (2001).
- ⁴ Nicola Marzari, Arash A. Mostofi, Jonathan R. Yates, Ivo Souza, and David Vanderbilt, Rev. Mod. Phys. **84**, 1419 (2012).
- ⁵ AA Mostofi, JR Yates, G Pizzi, YS Lee, I Souza, D Vanderbilt, N Marzari, Comput. Phys. Commun. **185**, 2309 (2014)
- ⁶ D. H. Lee and J. D. Joannopoulos, Phys. Rev. B **23**, 4988 (1981).
- ⁷ D. H. Lee and J. D. Joannopoulos, Phys. Rev. B **23**, 4997 (1981).
- ⁸ M P Lopez Sancho, J M Lopez Sancho, J M L Sancho and J Rubio, J. Phys. F:Met. Phys. **15**, 851 (1985).
- ⁹ QuanSheng Wu, ShengNan Zhang, Hai-Feng Song, Matthias Troyer, Alexey A. Soluyanov, Computer Physics Communications **224**, 405 (2018).
- ¹⁰ The Mathematical Theory of Symmetry in Solids: Representation Theory for Point Groups and Space Groups, P. Cracknell and Christopher J. Bradley, ISBN: 9780199582587, Oxford: Clarendon Press, 1972.
- ¹¹ B. Bradlyn *et al.*, Science 353, aaf5037 (2016)
- ¹² We also have $S_{2y}S_3 = S_3S_{2x}S_{2y}$ at R point, but this does not give any strong condition about the generation of new states.
- ¹³ V.I. Larchev and S. V. Popova, Journal of the Less-Common Metals **87**, 53 (1982).
- ¹⁴ N. Audebrand, M. Ellner, and E. Mittemeijer, Powder Diffraction, **15**(2), 120 (2000).